

Influence of CO₂ and H₂S Concentration on Hydrogen Permeation Behavior of P110 Steel

Shuliang Wang¹, Liang Wang¹, Xueguang Liu^{1,3}, Mingyu Bao¹, Li Liu^{1,*}, Xin Wang^{1,*},
Chengqiang Ren^{1,2}

¹ School of Materials Science and Engineering, Southwest Petroleum University, Chengdu, China, 610500

² State Key Laboratory of Oil and Gas Reservoir Geology and Exploitation, Southwest Petroleum University, Chengdu, China, 610500

³ Petro China Southwest Oil & Gasfield Company, Chengdu, China, 610213

*E-mail: wsliang1465@126.com, xin.wang@swpu.edu.cn

Received: 17 July 2017 / Accepted: 5 September 2017 / Published: 12 October 2017

The effect of CO₂ and H₂S concentration on the electrochemical and hydrogen permeation behaviors of P110 steel was investigated separately. The results showed that the corrosion current density was enhanced, while the polarization resistance and charge-transfer resistance decreased as the concentration of CO₂ and H₂S increased. The variation rule of hydrogen permeation behaviors can be described below: the hydrogen diffusion coefficient had little changed, whereas both of the diffusible hydrogen concentration and the steady-state hydrogen permeation current density increased. The steady-state hydrogen permeation current density in H₂S environment was far greater than that in CO₂ environment, which was caused by the poisoning of H₂S. The relationship between the hydrogen diffusion coefficient and temperature can be described by Arrhenius equation according to the hydrogen permeation curves at different temperatures.

Keywords: Electrochemistry; Hydrogen Permeation; P110 Steel

1. INTRODUCTION

With the continuous exploitation of acidic oil and gas fields in recent years, CO₂ and H₂S corrosion has become one of the biggest challenges that constrain oil and gas exploitation [1]. Dissolution of CO₂ and H₂S in water makes the solution acidic, leading to gradual destruction of the Oil casing known as the acid corrosion. In the complex CO₂ and H₂S environment, because of the existence of secondary hydrolysis, the two organics first decompose to form carbonic acid and hydrogen sulphate that will also dissociate into HCO₃⁻, CO₃²⁻, HS⁻, S²⁻ and other solution ions [2,

3]. The difference between CO_2 and H_2S content will lead to their complex interaction, making the oil casing corrosion more serious. Types of corrosion include crevice corrosion [4], galvanic corrosion [5] and hydrogen damage. Among them the most damaging one is the hydrogen damage, which can be categorized as hydrogen-type corrosion and hydrogen embrittlement. The main source of hydrogen in the metal is from two sides: one is the internal hydrogen, which is the entering of hydrogen into the inside of the metal in the smelting, welding, pickling, electroplating, atmosphere heat treatment and cathodic hydrogenation process; the other is external hydrogen, that is, hydrogen or hydrogen generating gas (H_2S , CO_2 , etc.) by the corrosion of the cathode process introducing hydrogen [6]. The cathodic acid corrosion reaction is the main source of hydrogen production [7]. Inside the metal, the atomic interaction force is at balance, whereas on the surface, the coordination number of the atoms is smaller than that inside, so imbalance of the atomic interaction force appears owing to the surface energy. This unbalanced interaction forces can attract the heterogeneous atoms to the surface, which can degrade the metal surface energy (the system energy decreases). Thus the metal has a tendency to adsorb heterogeneous atoms. When hydrogen contacts with metal, clean metal surface M will adsorb H_2 to form H_2M , where M is the surface of the metal material. The difference between H_2M and free H_2 is that the adsorbed hydrogen H_2M will be easily decomposed into adsorbed atoms, i.e. HM. After desorption, H can enter into the interior of the metal [8]. Once hydrogen is absorbed, it will be detected at the gap or trapped at the defects such as grain boundaries, voids, and interfaces. The presence of hydrogen will increase the concentration of voids [9, 10]. The atomic hydrogen can diffuse through lattice or grain boundary. The hydrogen diffusing via the grain boundary is usually higher than that via the lattice. Very little content of hydrogen will lead to the hydrogen damage of stressed metal [11, 12]. When hydrogen enters the material, the forms in the metal may be: H, H^+ , H^- , H_2 , all of which will interact with the metal material, causing declined toughness, plasticity and other mechanical properties of the metal material [13]. Therefore in the course of service, hydrogen induced delayed fracture, limits the wide application of materials [14-16].

Structural defects in the steel can also trap hydrogen. Depending on their hydrogen binding ability, the traps may be reversible hydrogen trap or irreversible hydrogen trap. The presence of hydrogen traps will affect the diffusion efficiency of hydrogen [17]. Diffusion studies at low temperature is not widely reported, due to slow dynamics, but the diffusion of hydrogen in the metal is an exception, for that the hydrogen atoms are pretty small and have a higher mobility even at low temperatures [18].

With the increase in strength, the hydrogen embrittlement sensitivity of the material is generally increased. Thus high-strength steel containing a small amount of hydrogen may induce hydrogen embrittlement that is closely related to the diffusion rate and diffusion mechanism of hydrogen permeation process. Therefore, it is necessary to study the hydrogen content in a quantitative way in the study of hydrogen permeation behavior. Up to date, there is little literature on the hydrogen permeation of the specific P110 steel in CO_2 and / or H_2S environments, yet, P110 steel is often used for well casing material in the offshore oil and gas industry [9]. Therefore, it is of great practical significance to study the hydrogen permeation behavior of P110 steel in $\text{H}_2\text{S}/\text{CO}_2$ environment. In this work, the electrochemical corrosion mechanism and hydrogen permeation behavior of P110 steel

under different H₂S/CO₂ concentration were studied. The effect of temperature on the hydrogen permeation curve of P110 steel in saturated H₂S/CO₂ solution was also demonstrated.

2. EXPERIMENTAL

2.1. Materials and environment

P110 steel, with chemical compositions(wt.%) C 0.26, Si 0.25, Mn 1.71, Ni 0.02, Cr 0.05, Mo 0.01, Ti 0.01 and Fe 97.69, was cut to square of 10 mm × 10 mm × 2mm ((L×W×H) and round plates of Φ45 mm × 0.5 mm. The square sample is used for electrochemical test, while the round plates whose effective area is 6.6 cm² is used as permeation hydrogen. The surface were polished with silicon carbide paper, degreased with acetone, washed in distilled water, and rinsed by alcohol followed by drying with N₂.

Experimental medium was prepared as follows. A NaCl of 3.5 wt. % was first prepared with distilled water, followed by deoxygenation with high purity N₂ for an adequate period of time (more than 8 h) while maintaining the concentration at 3.5 wt. %. High purity H₂S and CO₂ were then ventilated to the solution until saturation, give rise to the parent solution. A series of H₂S and CO₂ solutions with different concentration were prepared by mixing the neat 3.5 wt. % NaCl solution with the parent solution, as shown in Table 1. The temperature of the hydrogen permeation in saturated CO₂/H₂S solutions were 25 °C, 40 °C, 55 °C and 70 °C respectively.

Table 1. The configured experimental solutions with CO₂ and H₂S concentration

Experimental medium	1	2	3	4	5	6
H ₂ S(mmol·L ⁻¹)	0	20	40	60	80	100
CO ₂ (mmol·L ⁻¹)	0	8	16	24	32	40

2.2. Electrochemical measurement

An autolab Model PARSTAT 2273 Electrochemical Workstation was used for electrochemical measurements with three electrode cells, including a platinum plate counter-electrode, a saturated calomel reference electrode inserted in a electrolytic bridge and a specimen of P110 working electrode. Potentiodynamic polarization curves were acquired by varying the electrode potential from -300 mV to 300 mV over the corrosion potential(E_{corr}) at a scan rate of 1 mV/s. Electrochemical Impedance Spectroscopy(EIS) measured at a frequency range from 100 kHz to 0.00001 kHz under potentiodynamic conditions with an AC amplitude of 10mV at open potential.

2.3. Permeation hydrogen test

The double electrolytic cell of Devanathan-Stachurski, where the two sides of the round sample are two electrolytic cells isolated from each other, was utilized to research the permeation hydrogen

behavior of P110 steel. The left side of the equipment is used as the hydrogen filling anode chamber while the right side is used as the hydrogen diffusion cathode chamber [19].

Anode of the sample was plated with nickel at a current density of $10 \text{ mA}\cdot\text{cm}^{-2}$ in the Watt nickel plating solution ($215 \text{ g}\cdot\text{L}^{-1} \text{ NiSO}_4\cdot 6\text{H}_2\text{O}$, $11 \text{ g}\cdot\text{L}^{-1} \text{ NaCl}$, $33 \text{ g}\cdot\text{L}^{-1} \text{ H}_3\text{BO}_3$, $25 \text{ g}\cdot\text{L}^{-1} \text{ Na}_2\text{SO}_4$, $35 \text{ g}\cdot\text{L}^{-1} \text{ MgSO}_4$) for 5 minutes continuously before measurements.

A NaOH solution of $0.2 \text{ mol}\cdot\text{L}^{-1}$ was added to the anion chamber, then a 200 mV anode potential was applied by the Electrochemical. When the background current density is less than $1 \mu\text{A}\cdot\text{cm}^{-2}$, the solutions in Table 1 were injected into the cathodic chamber immediately, while the cathode surface of the sample was applied with a current density of $0.5 \text{ mA}\cdot\text{cm}^{-2}$ by a Model ZF-9 constant potential instrument. When the anode potential was kept as a constant, the hydrogenation current-time variation (permeation hydrogen curve) would be recorded until the current reached a steady state.

The most commonly used equations are equation (1) for hydrogen diffusion coefficient (D) and equation (2) for adsorption of hydrogen concentration (C_0) which can be calculated from the permeation hydrogen curve, according to Fick's laws of diffusion,

$$D = \frac{L^2}{6t_{0.63}i_{\infty}} \quad (1)$$

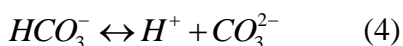
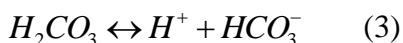
$$C_0 = \frac{i_{\infty}L}{FD} \quad (2)$$

where L is thickness (cm) of the sample (cm), i_{∞} is the steady current density of permeation hydrogen ($\mu\text{A}\cdot\text{cm}^{-2}$), $t_{0.63}$ is the time when current density is 0.63 times of i_{∞} (s), and F is the Faraday constant ($96485 \text{ C}\cdot\text{mol}^{-1}$).

3. RESULTS AND DISCUSSION

3.1. Influence of CO_2 concentration on the Electrochemical and Hydrogen Permeation Behavior of P110 Steel

CO_2 dissolved in water will produce carbonic acid, a dibasic acid, whose ionization is divided into two steps [2, 20, 21],



where the dissociation constant of the first step k_1 is 4.30×10^{-7} , and the second step k_2 is 4.30×10^{-11} . Because k_2 is too small compared to k_1 thus negligible reaction dissociation, it is often considered that only the first step of ionization occurs after CO_2 being dissolved in water. Then the three ions of H_2CO_3 , HCO_3^- , and H^+ would exist in the solution, whose concentrations would be increased with the increase of the CO_2 solubility, and consequently the decrease of the pH value.

The polarization curves in different CO_2 concentration condition are shown in Fig. 1. The corresponding electrochemical parameters after fitting are shown in Table 2. When the solution has no CO_2 , E_{corr} is -740.37 mV . At a CO_2 concentration of $8 \text{ mmol}\cdot\text{L}^{-1}$, E_{corr} becomes -719.3 mV . With the increase of CO_2 concentration, the probability of the binding of HCO_3^- to Fe^{2+} in solution increases. In other words, the concentration of Fe^{2+} on the surface decreases. In corrosive environment with the same pH value and cathode starting potential, the decrease of the Fe^{2+} concentration on the electrode

surface makes the anode starting potential even more negative, causing the anode polarization curve to move toward the negative direction, that is, the E_{corr} of metal moves to the negative direction. Veloz [22] found that in the same acidic solution, E_{corr} in the solution containing Cl^- is more positive than that in the solution without Cl^- . The addition of CO_2 makes the E_{corr} shift, which may be because that the CO_2 and the Cl^- form a competitive adsorption on the steel surface, leading to the increase in Fe^{2+} and therefore a small positive shift of E_{corr} . With the concentration increase of CO_2 in the solution, the impact of CO_2 on the open-circuit potential becomes small.

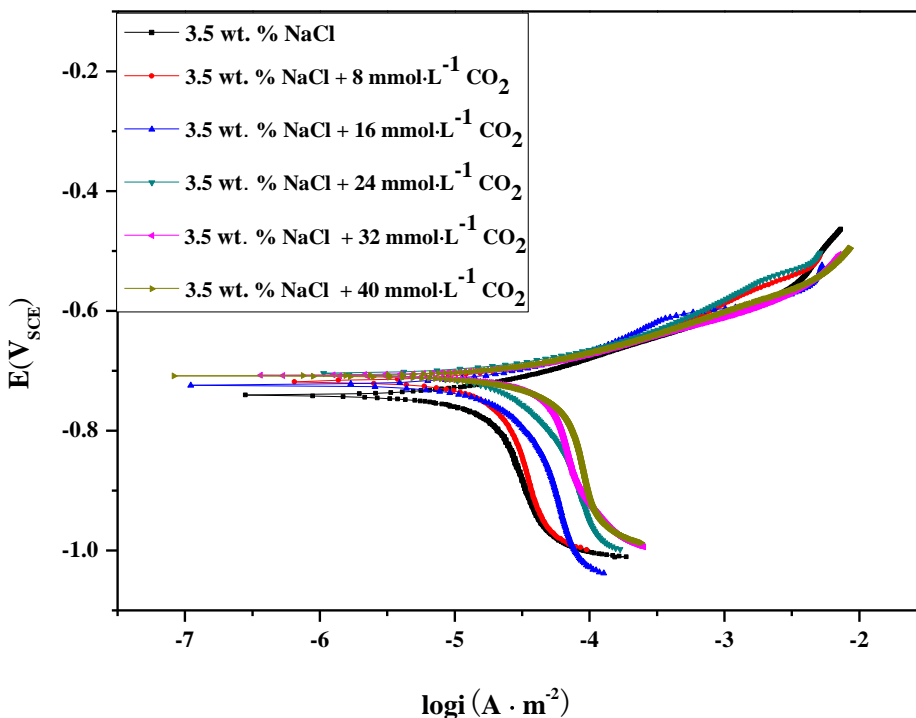


Figure 1. Polarization curves of P110 steel in solutions with different CO_2 concentration.

Table 2. Electrochemical parameters of the polarization curves of P110 steel at different CO_2 concentration.

CO_2 ($mmol \cdot L^{-1}$)	E_{corr} (mV)	b_a ($mV \cdot dec^{-1}$)	b_c ($mV \cdot dec^{-1}$)	i_{corr} ($\mu A \cdot cm^{-2}$)	R_p ($\Omega \cdot cm^2$)
0	-740.37	75.41	493.71	17.29	1672.06
8	-719.30	104.89	582.58	32.68	1233.24
16	-724.30	102.25	381.61	36.87	1115.83
24	-706.48	115.43	306.92	43.17	904.34
32	-707.26	100.43	795.79	50.633	759.19
40	-708.62	84.00	751.10	55.84	603.95

The polarization curves in Figure 1 have generally the same trend. When the polarization potential reaches E_{corr} , the anodic reaction current density of each curve increases with the increase of electrode potential, and the passivation phenomenon does not appear. P110 steel is in an activated

dissolved state at this time. However, with the increase of CO_2 concentration, the cathode part is shifted to the right, which maybe because of the increase of CO_2 concentration and the decrease of the pH of the solution. This promotes the cathodic reaction. However, the CO_2 concentration has little influence on the anodic polarization curves. The anode part of the curves are almost overlapping, indicating that the reaction mechanism of the anode part is the same. Yin [23] studied the polarization curve of P110 steel at different temperatures in a simulated oilfield solution containing CO_2 , and a similar situation occurred in the anode section, which is well consistent with the finding of this paper. The slope of the cathode Tafel (b_c) is greater than the anode Tafel slope (b_a), which indicate that the cathodic process is more hindered than the anode process, the whole reaction is controlled by the cathode, and the entire cathode part exhibits diffusion control. The theoretical b_c slope of the H^+ discharge process is $107.9 \text{ mV} \cdot \text{dec}^{-1}$, but the b_c of the polarization curves in this study are larger than this value, indicating that the cathodic reaction of P110 steel is not dominated by H^+ discharge in this environment. The study of Videm [24] suggests that the excess b_c is due to the fact that the electroactive substances participates in heterogeneous hydration adsorption on the electrode surface. According to the experimental conditions in the present work, H^+ , H_2CO_3 and HCO_3^- should be involved in the cathodic reaction. With the increase of CO_2 concentration, more H^+ , H_2CO_3 and HCO_3^- are involved in the cathodic reaction. That leads to steeper the cathode polarization curves are, as well as more obvious diffusion characteristics.

Figure 2 shows the influence of different CO_2 concentration on the self-corrosion current density (i_{corr}) and polarization resistance (R_p). It is found that with the increase of CO_2 concentration, i_{corr} increases from $17.29 \mu\text{A} \cdot \text{cm}^{-2}$ to $55.84 \mu\text{A} \cdot \text{cm}^{-2}$, while R_p decreases from $1672.06 \Omega \cdot \text{cm}^2$ to $603.95 \Omega \cdot \text{cm}^2$. This shows indicating that with the increase of CO_2 concentration, the reaction rate of the whole electrode system and the ion concentration involved in the cathodic reaction are increased, resulting in the increase in the cathode reaction rate.

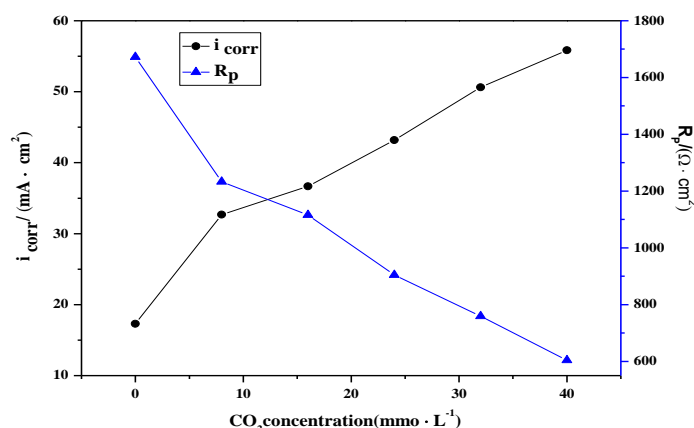
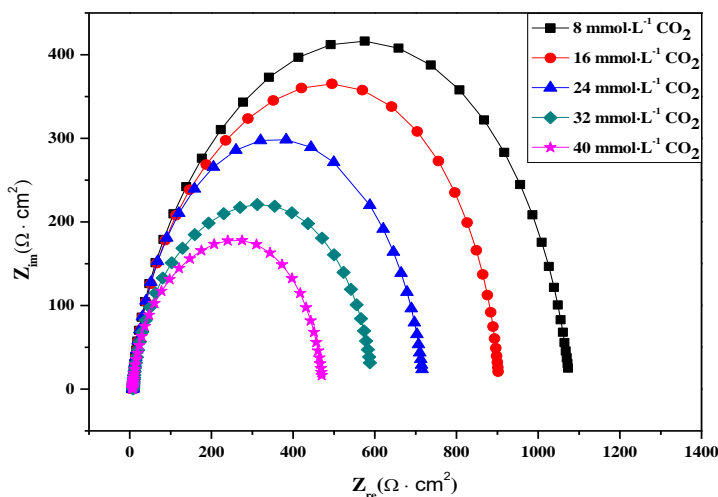


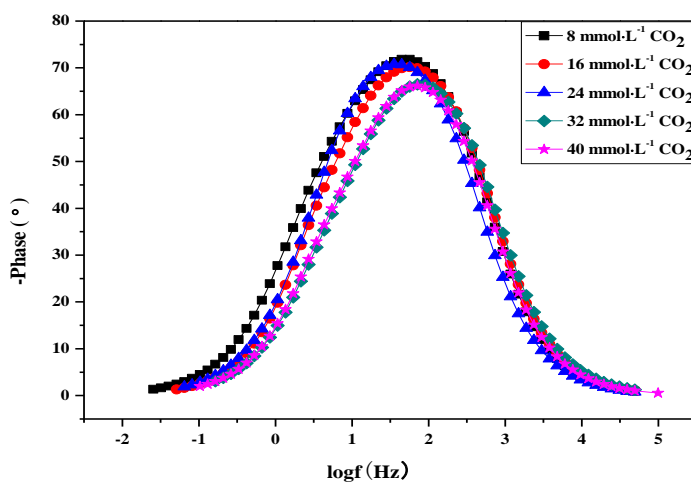
Figure 2. Value of i_{corr} and R_p of P110 steel at different CO_2 concentration.

The Nyquist and Bode plots of P110 steel at different CO_2 concentrations are shown in Fig. 3. The Nyquist and Bode graphs show that the EIS curves have only one time constant and that the Nyquist graph is presented as an integrated capacitive reactance arc. Since the P110 steel is in the

initial stage of immersion in different CO₂ concentration solutions, the surface of the steel is in an active state without corrosion product film, and the speed of the electrode reaction of the P110 steel is affected by at least two state variables, one of which is the electrode potential, and the other may also be the concentration of the reactants in the solution near the surface of the electrode. Therefore, the capacitive arc is related to the electric double layer capacitance and the reaction transfer resistance. The concentration of the reactants in the solution will affect the interface of the electric double layer, which is manifested as the change of the size of the resistive arc radius.



(a) Nyquist plot

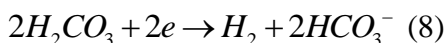
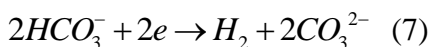
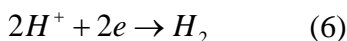


(b) Bode plot

Figure 3. EIS of P110 steel in solutions at different CO₂ concentrations: (a)Nyquist plot, (b) Bode plot.

With the increase of CO₂ concentration, the corresponding radius of the capacitive arc decreases. In the Bode graph, the phase angle peak gradually moves toward high frequency, with the

maximum of phase angle becomes smaller. Because CO_2 is dissolved in water, there will be H_2O , H^+ , HCO_3^- , H_2CO_3 and other cathode reducing substances. The cathode reaction process may exist the following reactions [25, 26],



Chen [27] found that the above four reactions can be carried out in CO_2 solution by thermodynamics calculation, and the velocity steps of these reactions are mainly affected by the concentration of the reactants. The reduction of H^+ in the above reaction is controlled by diffusion, while the residual reactions are controlled by activation. Nescic [20] summarized the corrosion reactions in the CO_2 environment and found that: only when the pH of the solution is less than 4, the cathodic process is dominated by H^+ reduction. However, when the pH of the solutions vary from 4 to 6, the reduction of H_2CO_3 and HCO_3^- is the main. When pH is high, the reduction of HCO_3^- in the CO_2 solution becomes very important [28]. The concentration of HCO_3^- also increases due to the increase in pH, making it difficult to distinguish reactions (7) and (8) from the path of hydrogen formation. Nescic studied the corrosion of CO_2 at different gas concentration by adjusting the pH of the saturated CO_2 solution. However, the pH value of the solutions with different concentration of CO_2 are between 4 and 6, and the EIS pattern only has the capacitive resistance characteristic, with no diffusion characteristic Warburg impedance appear. This clearly indicates that the reaction process is mainly controlled by activation, where more H_2CO_3 and HCO_3^- are involved in the cathodic reduction reaction, and H^+ is not the primary reactant.

Table 3 lists the calculated results of the various electrochemical parameters. The equivalent circuit diagram under this condition is shown in Fig. 4, where R_s is the solution resistance, and Q_{dl} is the electric double layer capacitance, and n is the dispersion index, and R_t is the charge transfer resistance [29].

Table 3. EIS parameters of P110 steel in solutions at different CO_2 concentration

CO_2 ($\text{mmol}\cdot\text{L}^{-1}$)	R_s ($\Omega\cdot\text{cm}^2$)	Q_{dl} ($\Omega^{-1}\cdot\text{cm}^{-2}\cdot\text{s}^{-n}$)	n	R_t ($\Omega\cdot\text{cm}^2$)
8	7.935	6.353×10^{-5}	0.928	1071.9
16	7.583	6.588×10^{-5}	0.912	894.3
24	7.331	7.154×10^{-5}	0.916	712.4
32	6.845	8.464×10^{-5}	0.902	587.4
40	6.742	9.421×10^{-5}	0.907	466.0

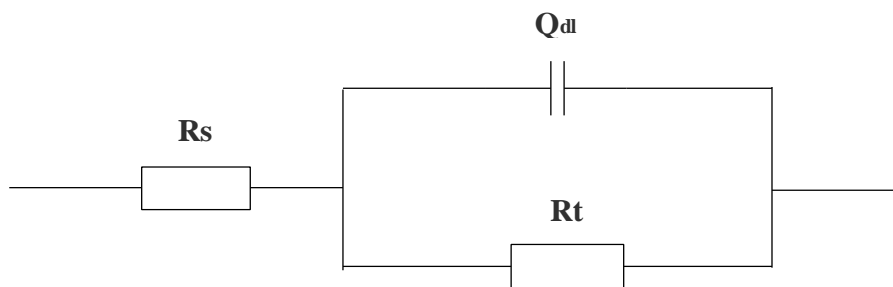


Figure 4. Equivalent circuit diagram of P110 steel in solutions at different CO₂ concentration as shown in Fig. 3.

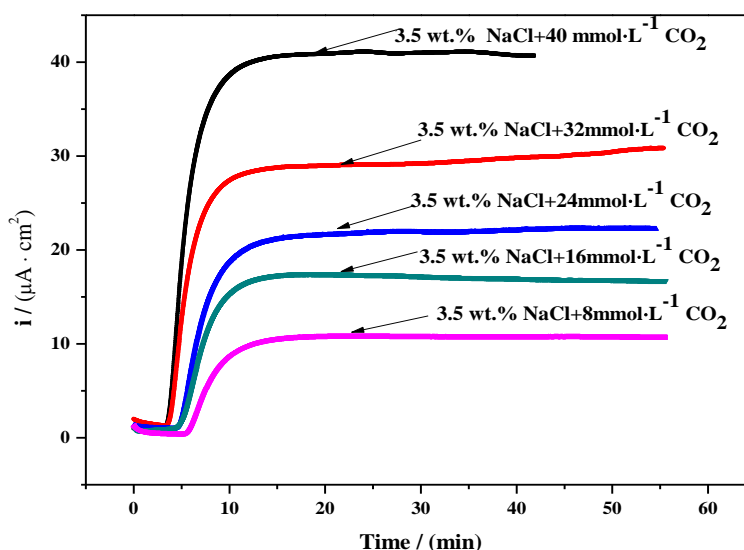


Figure 5. Hydrogen permeation curves of P110 steel at different CO₂ concentration

With the increase of the concentration of CO₂ in the solution, the pH value of the solution decreases and the R_s decreases subsequently. Meanwhile, the reaction of the whole electrode is promoted, So that the transfer process of charge passing through the two-phase interface of electrode and electrolyte solution is easier. As a result, the electric double layer capacitance Q_{dl} increases, and the charge transfer resistance R_t decreases. H₂CO₃, HCO₃⁻ and other ions that are involved in the cathodic reduction reaction are also increased in number, which are adsorbed at the electrode/solution interface and occupy more active sites, making the activation energy of the reaction even lower, and R_t smaller.

The hydrogen permeation curves of P110 steel in different CO₂ solutions are shown in Fig. 5. The relevant parameters calculated using the lag time method from hydrogen permeation curves in Figure 5, according to the equations (1) and (2), are shown in Table 4.

Table 4. Hydrogen permeation parameters at different CO₂ concentration

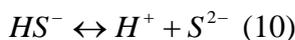
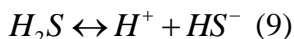
CO ₂ (mmol·L ⁻¹)	<i>D</i> (cm ² ·s ⁻¹)	<i>i</i> _∞ (μA·cm ⁻²)	<i>C</i> ₀ (μmol·cm ⁻³)
8	8.112×10 ⁻⁷	10.69	6.83
16	8.316×10 ⁻⁷	16.99	10.58
24	9.285×10 ⁻⁷	22.26	12.42
32	1.142×10 ⁻⁶	30.85	13.99
40	1.208×10 ⁻⁶	40.68	17.45

The penetration time (t_b) and steady current density (i_∞) decrease with the increase of the CO₂ concentration in the solution. The value of t_b is 306 s in the solution at CO₂ concentration of 8 mmol·L⁻¹, but was only 180 s in the solution at 40 mmol·L⁻¹. Besides the hydrogen permeation curves are shortened from the background current stage to the steady current stage. That is to say, the slope of the rising stage of the hydrogen permeation curves become larger, indicating that the time of hydrogen permeation curve need to reach the steady current is gradually shortened with the increase of the CO₂ concentration in the solution. In other words, the hydrogen permeation rate is gradually accelerated. Plennevaux [30] found that the presence of CO₂ in the solution promoted the entering of H into the metal and increased the efficiency of hydrogen permeation. Some previous studies [31, 32] have shown that hydrogen permeation rate is only related to the concentration of hydrogen in the solution, whereas in the present work, hydrogen is derived from aqueous CO₂. Therefore, the accelerated rate of hydrogen permeation is mainly because of two reasons. On one hand, the increase of CO₂ concentration and hydrogen evolution rate will lead to an increase of H⁺ concentration, which provide more hydrogen source to the cathode side. As a result, i_∞ gradually increases, and more hydrogen sources will lead to a larger hydrogen concentration gradient on both sides of the anode and cathode, resulting in a greater hydrogen diffusion rate; On the other hand, the influence of CO₂ on the cathode mainly depends on the mass transfer and dissociation process of H₂CO₃ in the solution, which will result in a larger cathode current [33]. Secondly, due to the buffering effect, H₂CO₃ will act as an additional useful proton container for chemical dissociation of steel surfaces that can facilitate the dissociation reaction and lead to a greater i_∞ [30].

The difference between the different concentration of the solutions is the pH value, and D , i_∞ and C_0 will increase with the increase of the solution concentration, indicating that the lower pH will be more conducive to the diffusion of hydrogen. There are two main factors affecting the hydrogen diffusion coefficient. First is the nature of the material itself, such as composition, structure and crystal defects; The diffusion activation energy of hydrogen in different metals is different, causing a difference in the diffusion coefficient of hydrogen up to several orders of magnitude [34]. The stress filed in the hydrogen atoms also interacts with defects in the crystal, impurity elements. Which hinders the movement of hydrogen atoms at different gap positions, thus results in a decrease in the hydrogen diffusion coefficient. Second is the measurement parameters, such as temperature, sample thickness, surface state, and the hydrogen concentration on the cathode, etc [35].

3.2. Effect of H₂S Concentration on the Electrochemistry and Hydrogen Permeation Behavior of P110 Steel

H₂S is an acid gas that is slightly soluble in water and act as a weak acid [36-38]. The two dissociation reactions of H₂S in water are,



where the dissociation constant of the first step k_1 is 9.10×10^{-8} , and of the second step k_2 is 1.10×10^{-12} . The k_2 in the second step is too small that is negligible. That is to assume that only the first step of ionization occurs after H₂S being dissolved in water, which means the concentration of S²⁻ in the solution is about 0, and the solution contain H₂S, HS⁻, and H⁺. With the increase of H₂S concentration, the concentration of these three ions will also increase. Because the increase of H⁺ concentration will result in the decrease of pH of solution, the first step dissociation reaction will be inhibited, and the growth rate of HS⁻ will become slow, even at high concentrations.

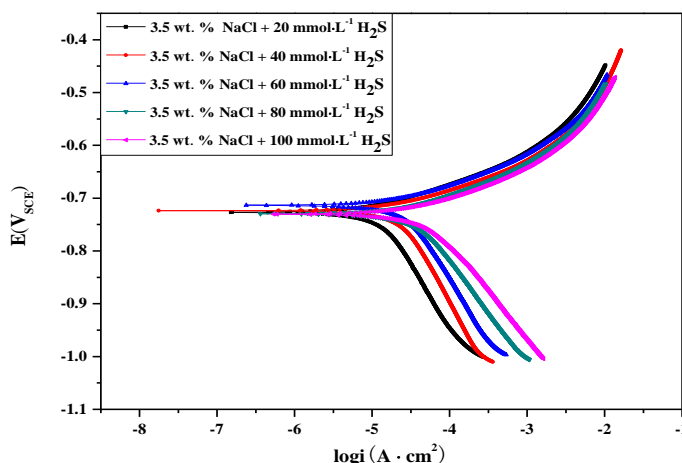


Figure 6. Polarization curves of P110 steel at different H₂S concentration

The polarization curves of P110 steel in H₂S solutions with different concentration are shown in Fig. 6. According to the electrochemical theory, the corrosion potential of P110 steel in acid H₂S medium should be in a mixed potential of Fe anodic dissolution and H⁺ reduction reversible potential interval. The H₂S concentration in the solution will mainly affect the reversible potential of the steel, but it will also affect the pH value of the solution. Therefore, it can be seen from the Figure 6 that the effect of the H₂S concentration on the corrosion potential is not significant. The overall trend of each curve is similar, and the steel is in an activated state and does not appear the passivation area in H₂S environment. It is obvious that the concentration of H₂S becomes larger and the cathode part of the polarization curves moves to the right. In other words, the concentration of H₂S in the solution becomes higher that promote the cathode reaction process. Feng [39] found that the presence of H₂S increased the anode and cathode current densities and suggested that the presence of HS⁻ provided additional H⁺ to promote the anodic reaction, and the increase in cathode current density was due to that H₂S was the main factor for hydrogen reduction reactant. In this study, H₂S is the main reactant.

The increase of the H₂S concentration will result in the increase of the H⁺ concentration gradient in the solution so that the rate of H⁺ migration from the solution near the electrode to the electrode surface is accelerated, thus contributing to the rate of cathodic hydrogen evolution reaction, causing the cathode reaction process to be accelerated.

Table 5. Electrochemical parameters of potential curves of P110 steel at different H₂S concentration

H ₂ S (mmol·L ⁻¹)	E_{corr} (mV)	b_a (mV·dec ⁻¹)	b_c (mV·dec ⁻¹)	i_{corr} (μA·cm ⁻²)	R_p (Ω·cm ²)
20	-727.11	108.27	258.97	34.93	950.46
40	-723.71	104.18	271.21	39.91	820.01
60	-713.28	107.36	243.57	44.69	724.97
80	-729.70	117.74	204.20	58.93	551.03
100	-729.95	112.68	186.18.	64.49	473.26

The Tafel regions of each curve were fitted to obtain the electrochemical parameters as shown in Table 5. The cathodic polarization curve of each curve is steeper than that of the anodic polarization curves. The value of b_c is larger than b_a , indicating that the cathode process is more blocked than the anode process and the whole reaction is controlled by the cathode. When the concentration of H₂S is 20 mmol·L⁻¹, the cathode part is slightly diffused, whereas when the concentration of H₂S is increased gradually, the whole reaction process becomes electrochemical control step, which may be owing to the lower pH value leading to different levels of hydrogen evolution. HS⁻ that is ionized from H₂S will be adsorbed on the surface of the P110 steel, which will reduce the activation energy of the steel surface and make it more likely to lose electrons. This is seen as that with the H₂S concentration increases, the anode part slightly shift to the right. At the same time, it is found that HS⁻ will form a competitive adsorption with Cl⁻ on the electrode surface, and the binding energy of HS⁻-Fe adsorbate is much larger than that of Cl⁻-Fe adsorbate [40]. Therefore, HS⁻ will be more easily adsorbed on the steel surface and form a layer of sulfide film quickly. The presence of this film will be conducive to the depolarization process of H⁺ reduction and also promote the cathodic reaction [41]. After the potentiostatic polarization test, there was a layer of black corrosion products on the electrode surface of the sample, but the polarization curve did not show the obvious diffusion current characteristic, indicating that the corrosion product film was loose Porous and non-protective. The study of Smith [42] shows the same conclusion, i.e., in a sodium chloride solution, i_{corr} of solution with dissolved H₂S is almost twice that without H₂S, whereas the anode current density of the solution with H₂S is smaller than that of the solution without H₂S. This is because that there is a layer of black film formed on the surface of the electrode, but this layer is mainly composed of mackinawite and cubic ferrous sulfide which cannot form passivation film, allowing local corrosion of the surface to occur.

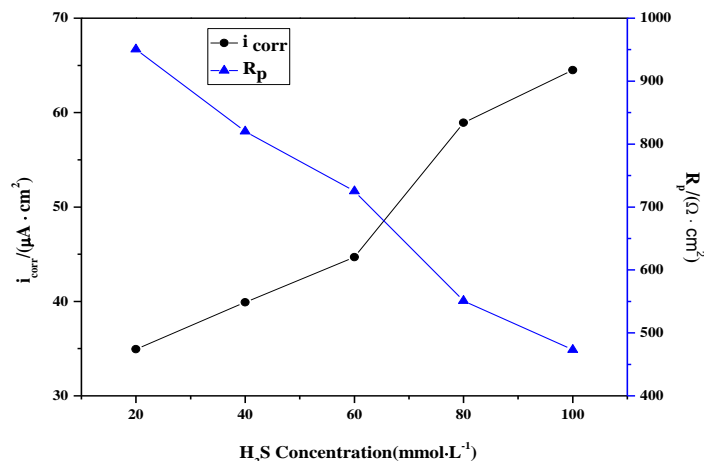
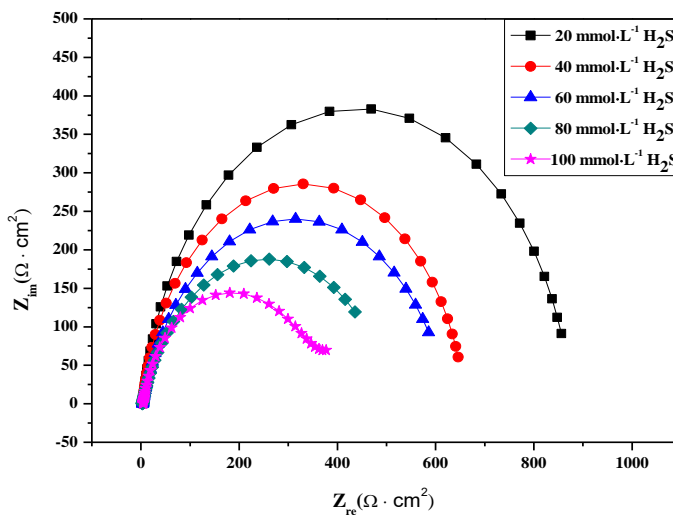


Figure 7. Value of i_{corr} and R_p of P110 steel at different H₂S concentration.

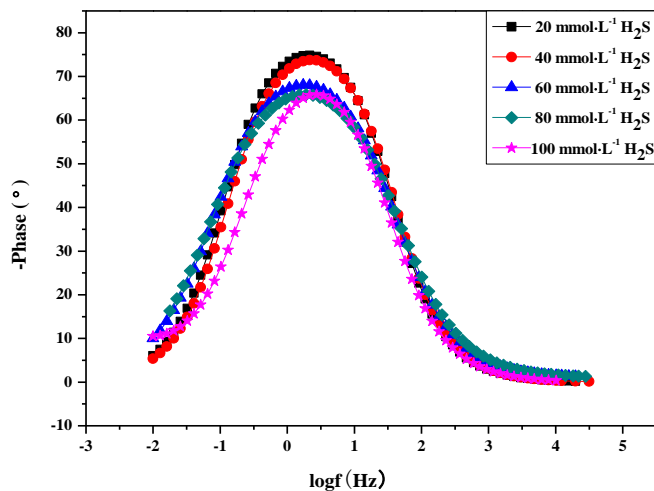
Figure 7 shows the effect of different H₂S concentration on i_{corr} and R_p . With the increase of H₂S concentration, i_{corr} increased from 34.93 $\mu\text{A}\cdot\text{cm}^{-2}$ to 64.49 $\mu\text{A}\cdot\text{cm}^{-2}$, while R_p decreased from 950.46 $\Omega\cdot\text{cm}^2$ to 473.26 $\Omega\cdot\text{cm}^2$. Ma [43] found that the addition of H₂S in the solution greatly accelerated the iron dissolution and cathodic hydrogen evolution reaction, the lower the pH, the more obvious the acceleration effect is. This shows that the rate of the whole electrode system reaction increases with the increase of H₂S concentration, which will lead to the decrease of the pH of the solution and provide more H⁺ for the reaction, thus increasing the cathode reaction rate.

By comparing H₂S with CO₂ at the same volume concentration, it was found that i_{corr} of P110 steel in H₂S solution was larger, and the R_p was smaller in H₂S solution. This may be due to the fact that the presence of H₂S increases the surface activity of P110 steel, as well as that the active position occupied by the Cl⁻ in CO₂ aqueous solution is more than that in H₂S aqueous solution, resulting in a decrease in the solubility of the CO₂ and a lower degree of corrosion.

The Nyquist and Bode plots of P110 steel at different H₂S concentration are shown in Fig. 8. The EIS curves has only one time constant and the Nyquist graph has a single capacitive arc. This is explained by taking account the corrosion reaction process. P110 steel in the solution of different H₂S concentration is merely at the initial stage of immersion that the surface of P110 steel is not covered by corrosion product film thus is in the activation state. Therefore, P110 steel electrode reaction has only one state variable, i.e. the electrode potential E. During the electrode reaction, C_{dl} is charged by the disturbance of the potential change and is restored to the initial state by the discharge of R_t . Together with the fact that the Warburg impedance is not shown in the EIS curve, it can be seen that there is no corrosion product film formed, and the ion diffusion and charge transfer process would not be hindered. With the increase of H₂S concentration, the corresponding radius of the capacitive arc decreases. In the Bode graph, the phase angle peak gradually moves toward high frequency region, and the maximum of phase angle becomes smaller. Although HS⁻ produced from H₂S is adsorbed on the electrode surface, there is only a single capacitive arc that is seen from the EIS curve. Therefore, it can be considered that the process is controlled by activation.



(a) Nyquist plot



(b) Bode plot

Figure 8. EIS of P110 steel in the solutions at different H₂S concentration: (a) Nyquist plot, (b) Bode plot.

Table 6. EIS parameters of P110 steel in the solutions of different H₂S concentration

H ₂ S (mmol·L ⁻¹)	R _s (Ω·cm ²)	Q _{dl} (Ω ⁻¹ ·cm ⁻² ·s ⁻ⁿ)	n	R _t (Ω·cm ²)
20	8.460	8.035×10 ⁻⁴	0.918	847.5
40	8.128	8.492×10 ⁻⁴	0.809	664.5
60	8.011	9.209×10 ⁻⁴	0.910	584.8
80	7.839	1.178×10 ⁻³	0.836	435.6
100	7.814	1.256×10 ⁻³	0.860	376.8

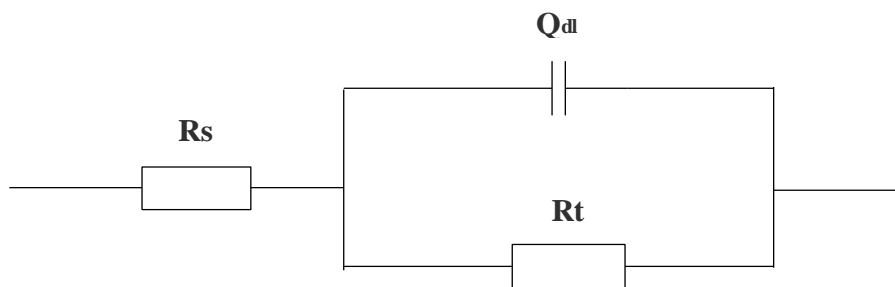


Figure 9. Equivalent circuit diagram of P110 steel in solutions of different H_2S concentration as shown in Fig. 8.

Table 6 lists the calculated values of the electrochemical parameters. The equivalent circuit diagram under this condition is shown in Fig. 9. With the increase of the concentration of H_2S in the solution, the pH value of the solution decreases and R_s decreases as well. Meanwhile, the reaction of the whole electrode is promoted, so that the transfer process of charge passing through the two-phase interface of electrode and electrolyte solution is easier, thus Q_{dl} increases, and R_t decreases.

The hydrogen permeation curves of the P110 steel in different H_2S solution are shown in Figure 10. The corresponding value are calculated based on equations (1) and (2) using the lag time method from hydrogen permeation curves in Figure 10, and are shown in Table 7. It is found that t_b was 252 s in the $20 \text{ mmol}\cdot\text{L}^{-1}\text{H}_2\text{S}$ solution, but was only 100 s in the solution of $100 \text{ mmol}\cdot\text{L}^{-1} \text{H}_2\text{S}$. With the increase of the H_2S solution concentration, t_b decreases and the slope of the hydrogen permeation curve becomes larger, which means that the hydrogen permeation rate also increases. In studying the effect of H_2S partial pressure on hydrogen permeation, Kappes [44] found that the corrosion product film formed on the steel surface had a hindrance to the movement of hydrogen into the metal body, and the increase of the hydrogen concentration enhanced the occupancy rate of the hydrogen trap and apparent diffusion coefficient, which is consistent with that of the study of Zhang [45]. Kappes qualitatively studied the effect of H_2S concentration on the hydrogen permeation in the solution, which was consistent with the quantitative results of the present study. When the H_2S concentration is greater than $60 \text{ mmol}\cdot\text{L}^{-1}$, i_∞ shows a trend from decline to rise. This may be because that, at the high concentration of H_2S , a layer of corrosion products film quickly forms on the steel surface and hinders the process of hydrogen permeation process. The reason for this may come from two aspects: on one hand, as the concentration of the H_2S increases, the dissociation causes H^+ concentration to increase, so does the pH of the solution, and provide more hydrogen; On the other hand, due to its poisoning effect, the presence of H_2S will facilitate the entering of hydrogen into the matrix. Although the specific explanation of the process is not clear, two general viewpoints were widely discussed [46-47]:

(1) S^{2-} ionized from H_2S causes the over-potential of molecular hydrogen increase in the metal, thereby hindering the escape of molecular hydrogen which is formed by the compounding of atomic hydrogen.

(2) H_2S is present in a molecular form, which acts as a bridge for H^+ discharge, thereby accelerates the discharge and increases the concentration of diffused hydrogen. HS^- that is dissociated from H_2S is strongly adsorbed on the surface of steel and adsorbs the hydrogen atoms on the steel

surface to form an intermediate product, thereby facilitating the entering of hydrogen atoms into the matrix.

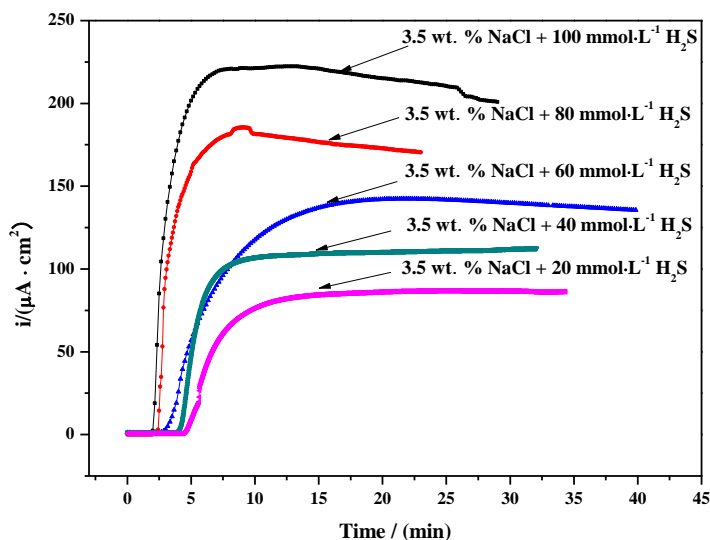


Figure 10. Hydrogen permeation curves of P110 steel at different H₂S concentration

It has been mentioned that the S²⁻ concentration in the solution is negligible and that a constant cathodic hydrogen charge current density is applied to the cathode side, which means that the H⁺ participating in the discharge per unit time is the same. Together with the specific experimental setup and detail, it is likely that point (2) is more reasonable for the present work. It is because of H₂S the poisoning effect of H₂S, that hydrogen atoms can be more readily adsorbed on the steel surface and further penetrate into the matrix. Therefore, compared with the CO₂ environment, the results obtained in H₂S showed higher *i_∞* and larger *C₀*.

Table 7. Hydrogen permeation parameters at different H₂S concentration

H ₂ S (mmol·L ⁻¹)	<i>D</i> (cm ² ·s ⁻¹)	<i>i_∞</i> (μA·cm ⁻²)	<i>C₀</i> (μmol·cm ⁻³)
20	1.002×10-6	86.31	44.63
40	1.053×10-6	112.55	55.38
60	1.124×10-6	135.65	62.53
80	1.187×10-6	170.43	74.39
100	1.237×10-6	200.93	84.16

3.3. Effect of temperature on hydrogen permeation behavior of P110 steel

Figure 11 shows the hydrogen permeation curves of P110 steel under different temperature gradient in saturated CO₂ environment. The corresponding values, shown in table 8, are calculated using the lag time method from hydrogen permeation curves in Figure 11, based on equations (1) and (2). It can be seen that *t_b* in the process of hydrogen permeation is obviously reduced with the increase

of experimental temperature. The slope of the hydrogen permeation curve before reaching i_{∞} gradually increases, indicating that the increase of temperature will accelerate the rate of hydrogen diffusion. At the same time, as the temperature increases, the steady current density of permeation hydrogen increases. The value of i_{∞} at 25 °C is 40.48 $\mu\text{A}\cdot\text{cm}^{-2}$, but increases to 130.82 $\mu\text{A}\cdot\text{cm}^{-2}$ when the temperature rises to 70 °C. With the extended hydrogen permeation time, the hydrogen permeation current gradually decreased, and eventually stabilized at 82.01 $\mu\text{A}\cdot\text{cm}^{-2}$. On one hand, the increase of temperature will promote the electrochemical reaction of the anode process and the cathode process, with a greater effect in the latter than in the former. The rate of hydrogen evolution is increased, which directly leads to the increase of H^+ concentration in the solution and provides more hydrogen source for the cathode side. At the same time, the increase of temperature will accelerate the diffusion rate of hydrogen, so the slope of hydrogen evolution curves become larger and the steady current density of permeation hydrogen is higher. On the other hand, the hydrogen permeation curves first increases, followed by a decrease, and then stabilizes at 70 °C. This is probably attributed to the excessively high hydrogen permeation current density formed as a result of the high temperature at the initial stage which improved the reaction and the diffusion rate. However, with the extended time, the excessively adsorbed hydrogen at the cathode will compound into H_2 , reducing the hydrogen concentration on the steel surface. In addition, a gradually formed a layer of corrosion product film on the surface of steel, though not dense and uniform, will definitely act as physical obstacles, hindering the diffusion of H.

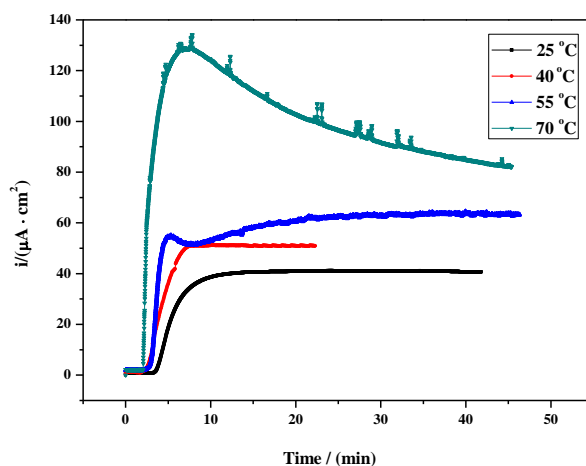


Figure 11. Hydrogen permeation curves of P110 steel in solutions containing saturated CO_2 at different temperatures

Table 8. The hydrogen permeation parameters of P110 steel in solutions containing saturated CO_2 at different temperatures

T (°C)	$t_{0.63}$ (s)	D ($\text{cm}^2\cdot\text{s}^{-1}$)	i_{∞} ($\mu\text{A}\cdot\text{cm}^{-2}$)	C_0 ($\mu\text{mol}\cdot\text{cm}^{-3}$)
25	345.00	1.208×10^{-6}	40.68	17.45
40	280.96	1.483×10^{-6}	50.95	17.80
55	233.20	1.786×10^{-6}	63.37	18.38
70	185.00	2.252×10^{-6}	82.01	18.86

The relationship between the hydrogen diffusion coefficient D and the temperature T can be expressed by the Arrhenius formula in the process of hydrogen permeation,

$$D = D_0 \exp\left(-\frac{E_a}{RT}\right) \tag{11}$$

where D_0 is the diffusion index ($\text{cm}^2 \cdot \text{s}^{-1}$), E_a is the diffusion activation energy ($\text{J} \cdot \text{mol}^{-1}$), R is the thermodynamic constants ($8.314 \text{ J} \cdot \text{K}^{-1} \cdot \text{mol}^{-1}$) and T is the temperature in Kelvin (K).

The above equation can be expressed as follow by taking natural logarithm on both sides.

$$\ln D = \ln D_0 - \frac{E_a}{RT} \tag{12}$$

According to the data in Table 8, $\ln D - T^{-1}$ is linear fitted, as is supported by a good linear relationship between the results of $\ln D$ and T^{-1} . The slope of the fitting is $-E_a/R$, and the intercept is $\ln D_0$. The undetermined coefficients can then be calculated, then the relationship between the diffusion coefficient D and the temperature in solutions containing saturated CO_2 can be obtained as follows.

$$D = 1.28 \times 10^{-4} \exp\left(-\frac{11606.34}{RT}\right) \tag{13}$$

Figure 12 shows the hydrogen permeation curves of P110 steel at different temperature gradients in saturated H_2S environment. Similar to the CO_2 environment, the hydrogen permeation curve becomes steeper as the temperature increases and the steady current density of permeation hydrogen also increases.

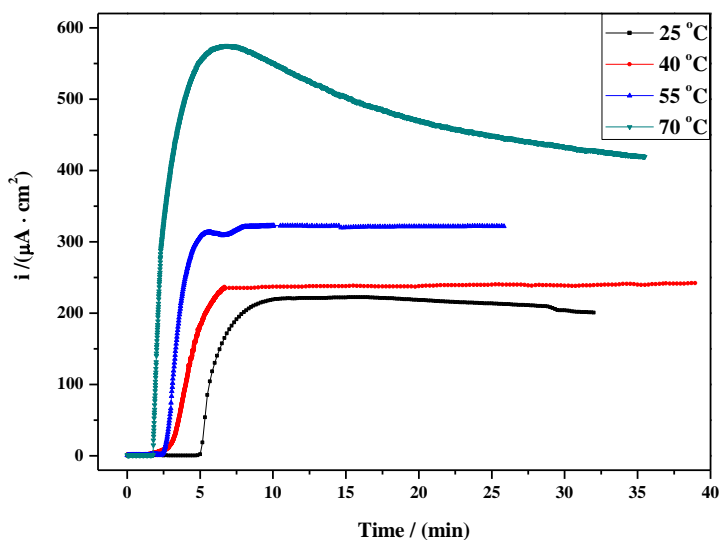


Figure 12. Hydrogen permeation curve of the P110 steel at different temperatures in saturated H_2S environment

The relevant parameters are calculated using the lag time method from hydrogen permeation curves in Figure 12, according to the equations (1) and (2), as shown in Table 9. The value of i_∞ is $200.93 \mu\text{A} \cdot \text{cm}^{-2}$ at $25 \text{ }^\circ\text{C}$, but reaches $548.12 \mu\text{A} \cdot \text{cm}^{-2}$ at $70 \text{ }^\circ\text{C}$, and then gradually decreases to $400.05 \mu\text{A} \cdot \text{cm}^{-2}$, which is nearly 2 times that at $25 \text{ }^\circ\text{C}$. This is because that, with the increase of temperature,

the kinetic energy of the diffusion of hydrogen atoms increases, resulting in an increase in the diffusion rate. Moreover the toxic effect of H₂S and rise of temperature promote the dissociation reaction, resulting in the increase of hydrogen concentration on the surface of the cathode. The Hydrogen atoms can then spread more quickly and efficiently in the steel. Meanwhile, the hydrogen permeation curve at 70 °C first increases, then decreases, and gradually stabilizes, which is also caused by the corrosion product film in this environment. Yang [48] found that the hydrogen diffusion coefficient increased with increasing temperature, which is consistent with the results of this study.

Table 9. Hydrogen permeation parameters at different temperatures in saturated H₂S environment

T (°C)	$t_{0.63}$ (s)	D (cm ² ·s ⁻¹)	i_{∞} (μA·cm ⁻²)	C_0 (μmol·cm ⁻³)
25	362.00	1.237×10 ⁻⁶	200.93	84.16
40	275.15	1.514×10 ⁻⁶	249.99	85.49
55	214.92	1.938×10 ⁻⁶	322.59	86.25
70	167.06	2.494×10 ⁻⁶	419.35	87.12

Similarly, the data in Table 9 shows that $\ln D-T^{-1}$ is linear fitted. Therefore, the relationship between the diffusion coefficient D and the temperature in solutions containing saturated H₂S can be obtained as follows:

$$D = 2.56 \times 10^{-4} \exp\left(-\frac{12981.86}{RT}\right) \quad (14)$$

4. CONCLUSIONS

In this paper, the electrochemical and hydrogen permeation behavior of the P110 steel at different concentration of CO₂ and H₂S were studied by electrochemical tests and hydrogen permeation experiments, and the influence of temperature on hydrogen permeation behavior was also investigated.

1. It was found that the overall trend of polarization curves of P110 steel were the same in the solutions with different CO₂ concentration, and the cathodic part is shown to be controlled by diffusion. However, cathodic part showed the electrochemical control step in different H₂S solutions. The polarization curves of CO₂ and H₂S solutions show the cathodic control step, and with the increase of the concentration, the self-corrosion current density increases, though the polarization resistance decreases.

2. The AC impedance spectra shows only one time constant at different concentration of CO₂ and H₂S, and the charge transfer resistance R_t decreases with the increase of the concentration.

3. The hydrogen permeation test shows that the hydrogen diffusion coefficient changes little in the solution of different concentration of CO₂ and H₂S, whereas the concentration of diffusible hydrogen and the steady current density of permeation hydrogen increased. Because of the poisoning

of H₂S, the steady current density of permeation hydrogen in H₂S environment is much greater than that in CO₂ environment.

4. Temperature is found to be the main influencing factor of hydrogen permeation. Based on the calculation of different hydrogen permeation parameters, the relationship between hydrogen diffusion coefficient and temperature is established. The hydrogen diffusion coefficient and the concentration of diffused hydrogen increased with the increase of temperature. The hydrogen diffusion coefficient and the concentration of diffused hydrogen increase with increasing temperature.

ACKNOWLEDGEMENTS

This work was financially supported by the National Natural Science Foundation of China (No. 51374180), National Undergraduate Training Program for Innovation and Entrepreneurship (201610615034). The authors also acknowledge a research funding from the Education Department of Sichuan Province (No. 17ZA0419).

References

1. G. A. Zhang, Y. Zeng, X. P. Guo, F. Jiang, D. Y. Shi and Z. Y. Chen, *Corros. Sci.*, 65 (2012) 37.
2. J. Kittel, F. Ropital, F. Grosjean, E. M. M. Sutter and B. Tribollet, *Corros. Sci.*, 66 (2013) 342.
3. B. Tribollet, J. Kittel, A. Meroufel, F. Ropital, F. Grosjean and E. M. M. Sutter, *electrochim. acta*, 124 (2014) 46.
4. C. Q. Ren, J. B. Chen, L. D. Pu, L. Liu, Y. Pan, J. Y. Hu and T. H. Shi, *Int. J. Electrochem. Sci.*, 10 (2015) 8210.
5. C. Q. Ren, M. Zhu, L. Du, J. B. Chen, D. Z. Zeng, J. Y. Hu and T. H. Shi, *Int. J. Electrochem. Sci.*, 10 (2015) 4029.
6. Y. M. Qi, H. Y. Luo, S. Q. Zheng, C. F. Chen, Z. G. Lv and M. X. Xiong, *Mater. Design*, 58 (2014) 234.
7. W. Y. Chu, S. Q. LI, C. M. HAIAO and J. Z. Tien, *Corrosion*, 36 (1980) 475.
8. M. Boudart, *J. Chem. Phys.*, 23 (1955) 753.
9. L. Simoni, J. Q. Caselani, L. B. Ramos, R. M. Schroeder and C. D. F. Malfatti, *Corros. Sci.*, 118 (2017) 178.
10. F. F. Dear and G. C. G. Skinner, *Phil. Trans. R. Soc. A*, 375 (2017) 20170032.
11. O. Kazum, H. Beladi, I. B. Timokhina, Y. He and M. B. Kannan, *Metall. Mater. Trans. A*, 47 (2016) 4896.
12. A. J. Haq, K. Muzaka, D. P. Dunne, A. Calka and E. V. Pereloma, *Int. J. Hydrogen. Energy*, 38 (2013) 2544.
13. P. Cotterill, *Prog. Mater. Sci.*, 9 (1961) 205.
14. W. Y. Chu, J. X. Li, C. H. Huang, Y. B. Wang and L. J. Qiao, *Corrosion*, 55 (1999) 892.
15. M. Kamilyan, R. Silverstein and D. Eliezer, *J. Mater. Sci.*, 52 (2017) 11091.
16. M. B. Djukic, V. S. Zeravcic, G. M. Bakic, A. Sedmak and B. Rajcic, *Eng. Fail. Anal.*, 58 (2015) 485.
17. B. A. Szost, R. H. Vegter and P. E. J. Rivera-Díaz-del-Castillo, *Metal. Mater. Trans. A*, 44 (2013) 4542.
18. H. Magnusson and K. Frisk, *J. Phase Equilib. Diff.*, 38 (2017) 65.
19. M. A. V. Devanathan, Z. Stachurski and W. Beck, *J. Electrochem. Soc.*, 110 (1963) 886.
20. S. Nešić, *Corros. Sci.*, 49 (2007) 4308.
21. B. R. Linter and G. T. Burstein, *Corros. Sci.*, 41 (1999) 117.
22. M. A. Veloz and I. González, *Electrochim. Acta*, 48 (2002) 135.
23. Z. F. Yin, X. Z. Wang, R. M. Gao, S. J. Zhang and Z. Q. Bai, *Anti-Corros. Method. M.*, 58 (2011)

227.

24. K. Videm, Fundamental studies aimed at improving models for prediction of CO₂ corrosion, Progress in the Understanding and Prevention of Corrosion, London, UK, 1993, p.513.
25. G. Zhang, C. Chen, M. Lu, C. Chai and Y. Wu, *Mater. Chem. Phys.*, 105 (2007) 331.
26. S. Nesic, J. Postlethwaite and S. Olsen, *Corros. Sci.*, 52 (1996) 280.
27. C. F. Chen, M. X. Xu, G. X. Xian, Z. Q. Bai, M. L. Yan and Y. Q. Yang, *Acta Metall. Sin.*, 39 (2003) 94.
28. L. G. S. Gray, B. G. Anderson, M. J. Danysh and P. R. Tremaine, Effect of pH and temperature on the mechanism of carbon steel corrosion by aqueous carbon dioxide, Corrosion/90, Houston, US, 1990, p.40.
29. Y. Chen and W. P. Jepson, *Electrochim. Acta*, 44 (1999) 4453.
30. C. Plennevaux, J. Kittel, M. Frégonèse, B. Normand, F. Ropital, F. Grosjean and T. Cassagne, *Electrochem. Commun.*, 26 (2013) 17.
31. F. Gallucci, F. Chiaravalloti, S. Tosti, E. Drioli and A. Basile, *Int. J. Hydrogen Energ.*, 32 (2007) 1837.
32. A. Unemoto, A. Kaimai, K. Sato, T. Otake, K. Yashiro, J. Mizusaki, T. Kawada, T. Tsuneki, Y. Shirasaki and I. Yasuda, *Int. J. Hydrogen Energ.*, 32 (2007) 4023.
33. E. Remita, B. Tribollet, E. Sutter, V. Vivier, F. Ropital and J. Kittel, *Corros. Sci.*, 50 (2008) 1433.
34. K. Kiuchi and R. B. McLellan, *Acta Metall. Mater.*, 31 (1983) 961.
35. T. Y. Zhang and Y. P. Zheng, *Acta Mater.*, 46 (1998) 5023.
36. R. H. Hausler, *Corrosion*, 54 (1998) 641.
37. J. I. Lee and A. E. Mather, *Ber. Bunsen-Ges. Phys. Chem.*, 81 (1977) 1020.
38. O. M. Suleimenov and R. E. Krupp, *Geochim. Cosmochim. Ac*, 58 (1994) 2433.
39. R. Feng, J. Beck, M. Ziomek-Moroz and S. N. Lvov, *Electrochim. Acta*, 212 (2016) 998.
40. L. J. Yan, L. Niu, H. C. Lin, W. T. Wu and S. Z. Liu, *Corros. Sci.*, 41 (1999) 2303.
41. F. Huang, P. Cheng, X. Y. Zhao, J. Liu, Q. Hu and Y. F. Cheng, *Int. J. Hydrogen Energ.*, 42 (2017) 4561.
42. P. Smith, S. Roy, D. Swailes, S. Maxwell, D. Page and J. Lawson, *Chem. Eng. Sci.*, 66 (2011) 5775.
43. H. Ma, X. Cheng, G. Li, S. Chen, Z. Quan, S. Y. Zhao and L. Niu, *Corros. Sci.*, 42 (2000) 1669.
44. M. Kappes, G. S. Frankel, R. Thodla, M. Mueller, N. Sridhar and R. M. Carranza, *Corros. Sci.*, 68 (2012) 1015.
45. X. Y. Zhang and Y. L. Du, *Br. Corros. J.*, 33 (1998) 292.
46. J. O'M. Bockris and H. Mauser, *Can. J. Chem.*, 37 (1959) 475.
47. A. Kawashima, K. Hashimoto and S. Shimodaira, *Corrosion*, 32 (1976) 321.
48. J. Y. Yang, C. Nishimura and M. Komaki, *J. Membrane. Sci.*, 309 (2008) 246.